Precision Medicine and Imaging

Clinical Cancer Research

Residual Tumor Volume, Cell Volume Fraction, and Tumor Cell Kill During Fractionated Chemoradiation Therapy of Human Glioblastoma using Quantitative Sodium MR Imaging

Keith R. Thulborn[1], Aiming Lu[1], Ian C. Atkinson[1], Mohan Pauliah[2], Kathryn Beal[3], Timothy A. Chan[3], Antonio Omuro[4], Josh Yamada[3], and Michelle S. Bradbury[2,5]

Abstract

Purpose: Spatial and temporal patterns of response of human glioblastoma to fractionated chemoradiation are described by changes in the bioscales of residual tumor volume (RTV), tumor cell volume fraction (CVF), and tumor cell kill (TCK), as derived from tissue sodium concentration (TSC) measured by quantitative sodium MRI at 3 Tesla. These near real-time patterns during treatment are compared with overall survival.

Experimental Design: Bioscales were mapped during fractionated chemoradiation therapy in patients with glioblastomas ($n = 20$) using TSC obtained from serial quantitative sodium MRI at 3 Tesla and a two-compartment model of tissue sodium distribution. The responses of these parameters in newly diagnosed human glioblastomas undergoing treatment were compared with time-to-disease progression and survival.

Results: RTV following tumor resection showed decreased CVF due to disruption of normal cell packing by edema and infiltrating tumor cells. CVF showed either increases back toward normal as infiltrating tumor cells were killed, or decreases as cancer cells continued to infiltrate and extend tumor margins. These highly variable tumor responses showed no correlation with time-to-progression or overall survival.

Conclusions: These bioscales indicate that fractionated chemoradiotherapy of glioblastomas produces variable responses with low cell killing efficiency. These parameters are sensitive to real-time changes within the treatment volume while remaining stable elsewhere, highlighting the potential to individualize therapy earlier in management, should alternative strategies be available.

Introduction

Glioblastoma is the most common malignant primary brain tumor in adults, classified as grade IV by the World Health Organization (WHO). This infiltrating astrocytic tumor retains an abysmal prognosis of less than 5% survival at 5 years (1, 2) despite decades of research and multiple clinical trials and despite trimodal treatment with surgery, radiation, and chemotherapy. Prognosis depends on clinical and genetic factors as well as extent of resection and adjuvant treatment (2, 3). However, glioblastoma is a heterogeneous entity with four genetically characterized subtypes (classical, mesenchymal, proneural, and neural) exhibiting different behaviors and treatment responses (4). Despite the genetic complexity, all glioblastomas are treated with the same protocol.

The infiltrating nature of this tumor has been known for decades (2, 5, 6). Pretreatment biopsies aligned with contrast-enhanced MRI images have shown that significant numbers of viable tumor cells infiltrate the nonenhancing tissue beyond the enhancing tumor (7). Such infiltrating behavior explains why residual tumor volume (RTV) has been reported as a better prognostic indicator than the extent of resection (8). The biology of glioblastoma has been reviewed elsewhere (6, 9, 10).

The low sensitivity of sodium MRI (11–16) required 3 Tesla clinical MR scanners (17) and efficient twisted projection imaging acquisitions (18) to make human applications feasible. The quantification of the MR signal was an important advancement to obtain metabolic information (19) that was validated in animal models of normal brain tissue (20) and brain tumors (21). Quantification has now been reported in human brain by a number of groups (reviewed in ref. 22).

Changes in tissue sodium ion concentration provide information about tissue viability and microstructure (19). The two-compartment model allows the MR-based measurement of tissue sodium concentration (TSC) to be interpreted as cell volume fraction (CVF), a tightly conserved parameter of adult brains across normal ageing (23). Tumors disrupt normal cell packing and have an expanded extracellular matrix with reduced CVF, as confirmed by a number of techniques (reviewed in refs. 21; 22).

[1]Center for Magnetic Resonance Research, University of Illinois at Chicago, Chicago, Illinois. [2]Department of Radiology, Memorial Sloan Kettering Cancer Center, New York, New York. [3]Department of Radiation Oncology, Memorial Sloan Kettering Cancer Center, New York, New York. [4]Department of Neurology, Memorial Sloan Kettering Cancer Center, New York, New York. [5]Molecular Pharmacology Program, Sloan Kettering Institute for Cancer Research, New York, New York.

Note: Supplementary data for this article are available at Clinical Cancer Research Online (http://clincancerres.aacrjournals.org/).

Corresponding Author: Keith R. Thulborn, University of Illinois at Chicago, OCC suite 1307, 1801 West Taylor Street, Chicago, IL 60612. Phone: 847-830-0725; Fax: 312-996-8305; E-mail: mrix@ameritech.net

doi: 10.1158/1078-0432.CCR-18-2079

Translational Relevance

Quantitative sodium MRI and the two-compartment model of sodium distribution in the brain provide biologically relevant objective measures of residual tumor volume (RTV), cell volume fraction (CVF), and tumor cell kill (TCK) in near real-time during chemoradiation of human glioblastomas. The variable responses and low efficiency of cell kill were not prognostic of survival time or time to first disease progression, but were consistent with the failure of this treatment and the need for subsequent treatment including multiple surgical resections. These parameters offer a means of tailoring patient management to real-time biological responses of tumors to treatment and may justify changing management if alternative treatments are available. These parameters may also offer better treatment outcome measures for clinical trials, measuring biological response of the tumor to the specific therapy, rather than its contribution to the global outcome of patient survival.

The difference in CVF between brain parenchyma and tumors provides an objective way to measure RTV as the infiltrated tissue surrounding the surgical resection site. As the measurements are quantitative, the temporal change in CVF within the changing RTV determines the tumor cell kill (TCK). The CVF of normal tissue away from the treatment site provides the internal control for the longitudinal reproducibility of the measurements.

Changes in RTV, CVF, and TCK bioscales during treatment as derived from TSC measurements from quantitative sodium MRI on a 3 Tesla clinical scanner are now reported for assessment of the therapeutic efficiency of intensity-modulated radiotherapy with concurrent temozolomide chemotherapy in the residual tumor bed following resection of human glioblastoma. These parameters indicate that this treatment produces highly variable TCK that does not correlate with survival. The low efficiency of TCK emphasizes the need for better treatment protocols.

Materials and Methods

Demographics

Patients ($n = 20$; age $= 58.6 \pm 8.6$ years) with new diagnosis of primary glioblastoma (WHO grade IV) signed consent forms approved by the Institutional Review Board using the rules of the Declaration of Helsinki, the Belmont Report, and the U.S. Common Rule for entry into this protocol for quantitative sodium MRI at 3.0 Tesla during chemoradiation treatment with clinical follow-up. All but 2 patients had undergone surgical resection shortly ($n = 18$, 35 ± 12 days) prior to radiation treatment and all were treated with fractionated radiation (60 Gy over 6 weeks delivered on 5 of 7 days with 2-Gy fractions with only small variations) with low-dose concurrent chemotherapy (temozolomide) given as per standard dosing schedule of 75 mg/m^2 daily. Tumors were distributed between the cerebral hemispheres (frontal 4, parietal 6, temporal 8, and occipital 2) without involving deep brain structures, brainstem, or cerebellum. Patients were followed until death with survival time (days) taken from the date of resection ($n = 18$) or first radiation treatment if not resected ($n = 2$). The Karnofsky performance scores (KPS) were assessed prior to radiation as greater than 70 for all subjects (KPS $= 87 \pm 10$). Only limited genetic marker results were available at the time of this study. The *MGMT* methylation status was negative for all but 4 participants. The *IDH1* status was negative for 15 participants and not tested in the remaining 5 subjects. The chemotherapy following radiation included adjuvant temozolomide (150–200 mg/m^2), but was variable across patients following recurrence, but most often included bevacizumab. Repeat resections were performed in some patients ($n = 8$).

Imaging protocol

All MRI was performed on a 3 Tesla clinical scanner (Signa HDx, GE Healthcare) equipped for sodium imaging and conventional multi-channel proton imaging. The sodium radiofrequency (RF) coil was a high-pass, single-tuned, quadrature, birdcage, and head volume coil (26 cm diameter, 8 rung) that could be exchanged, without moving the patient's head, with a geometrically identical proton RF coil that allowed B0 shimming and mapping to correct magnetic field inhomogeneities (24). Exchanging coils was accomplished using a cantilevered head support that was independent of the RF coils and yet centered the patient's head within the coils.

The three-dimensional (3D) flexible twisted projection imaging (flexTPI) provided an efficient acquisition pulse sequence with minimum time to echo (TE; 0.26 ms) in less than 10 minutes, as described elsewhere (24). Image reconstruction was performed after gridding the projection time domain data onto a Cartesian grid and fast Fourier transformation, as described in detail elsewhere (18, 24). The sodium signal quantification was performed using an imaging protocol that included B0 and B1 correction for the inhomogeneities in signal sensitivity across the field of view, described elsewhere (18, 24). The calibration phantom was a plastic sphere (16-cm diameter) containing three calibration cylinders (30, 70, 110 mmol/L NaCl in 3% agar surrounded by KCl, 60 mmol/L) that had the same electrical loading as a human head, and was imaged separately under the same imaging conditions as the patient.

The protocol over the 6-week chemoradiation treatment period included pre- and postradiation imaging examinations and between one to three additional imaging examinations during this period depending on patient tolerance (six studies in 1 patient, five studies in each of 2 patients, four studies in each of 9 patients, three studies in each of 7 patients, and two studies only in 1 patient).

Bioscale determination

Image processing was performed using customized software (MathLab R2015b) with B0 and B1 correction for both human and phantom images, followed by quantification by combining the linear three-point calibration from the phantom with the human images to obtain the TSC bioscale maps (19, 23). Bioscales from the multiple imaging sessions were aligned for each patient using a previously reported alignment strategy that avoids additional image blurring (25). Using the two-compartment model (22–24), the TSC maps were converted to CVF bioscale maps, as discussed below.

Bioscale analysis

Multiple ($n = 3$–6) TSC bioscale maps of each subject were analyzed for patterns of temporal and spatial changes during the course of radiation treatment using regions of interest (ROI) placed over the tumor and over normal brain tissue away from the treatment site to generate histograms of these regions. The

preradiation maps served as the baseline histograms for establishing the boundary threshold between normal tissue and the surgical bed. Descriptive statistics (mean, SD) established a filter range (filter range = 2SD, i.e., 24 < TSC < 44 mmol/L) for normal tissue (TSC mean = 34 ± 5 mmol/L) with a wider filter range (44 < TSC < 80 mmol/L) for tumor (TSC mean = 56 ± 4 mmol/L). This threshold of 44 mmol/L between tumor and normal parenchyma allowed RTV boundaries to be determined objectively within a rapidly selected ROI, without intensive manual segmentation. This boundary of two SDs (±10 mmol/L) from the mean value of normal tissue covered sites of likely progression as 90% of recurrence is within 2 cm of surgical margins (26).

The two-compartment model assumed intracellular and extracellular sodium concentrations of 12 mmol/L (C_i) and 145 mmol/L (C_e), respectively (22), such that:

$$CVF = \frac{(TSC - C_e)}{(C_i - C_e)} \quad (A)$$

Although proliferating cells have a higher intracellular sodium concentration than normal tissue, the resultant error is small (~3%) even after doubling this concentration. This small error reflects the much smaller intracellular concentration to the extracellular concentration (22). TCK maps were calculated as the fractional difference between the product of initial and final values of RTV (RTV_{Ti} and RTV_{Tf}, respectively) and CVF (CVF_{Ti} and CVF_{Tf}, respectively) divided by the product of the RTV_{Ti} and CVF_{Ti}.

$$TCK = \{(RTV_{Ti}.CVF_{Ti}) - (RTV_{Tf}.CVF_{Tf})\}/(RTV_{Ti}.CVF_{Ti}) = 1 - (RTV_{Tf}.CVF_{Tf})/(RTV_{Ti}.CVF_{Ti}) \quad (B)$$

When $RTV_{Tf}.CVF_{Tf} < RTV_{Ti}.CVF_{Ti}$, then $0 < TCK < 1$ and net tumor cells have been killed. However, when $RTV_{Tf}.CVF_{Tf} > RTV_{Ti}.CVF_{Ti}$, then $TCK < 0$, indicating that the tumor has progressed with a net gain of cells.

Statistical analysis

Linear regressions of changes in TSC, RTV, CVF, and TCK as a function of chemoradiation duration were performed separately for each patient. Patients were then divided into groups 1 and 2 based on decrease and increase in RTV across radiation treatment, respectively, as determined by the negative or positive Pearson coefficients of these regression analyses. Student *t* tests, (two-tailed, $P < 0.05$ for significance) were used to examine statistical significance of these Pearson coefficients and any differences between the two groups for each of the bioscales, time to first tumor progression, and survival. The mean CVF and any change in CVF during treatment in the normal brain away from the treatment site served as an internal control for the stability of the quantification methodology for each patient across multiple examination sessions. Additional correlations were examined between initial tumor RTV, CVF, and TCK and survival.

Bioscale modeling

The CVF of tumors is much lower than normal brain decreasing from normal tissue (CVF ~ 0.82) at the margin of the tumor to the center of the tumor (CVF ~ 0.55; ref. 27) as illustrated in Fig. 1. The RTV in the margin around a surgically resection is infiltrated by tumor cells, inflammation, and edema that disrupt normal cell packing (Fig. 1A). Surgical resection removes the bulk tumor leaving a cerebrospinal fluid (CSF)-filled cavity (Fig. 1B). The desirable response to fractionated chemoradiation treatment is killing of tumor cells with reduced inflammation and edema, resulting in CVF increasing back toward normal values (Fig. 1C) with a reduction in volume of the resection cavity. Unsuccessful treatment results in widening infiltration of the tumor that further lowers CVF and expands the RTV (Fig. 1D). Although peripheral

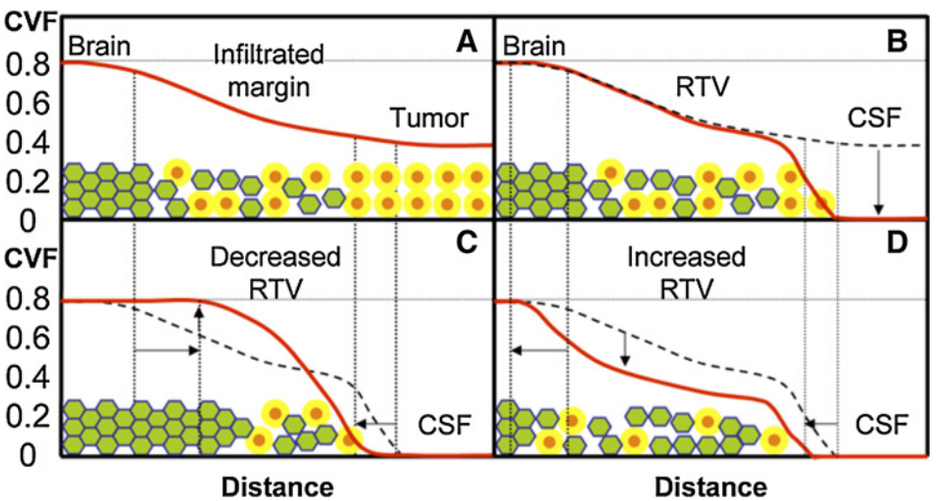

Figure 1.

Model for the profile (solid red line) of CVF from normal brain tissue through to the center of the glioblastoma. **A,** Prior to partial surgical resection, CVF in normal brain (CVF = 0.82) decreases through the infiltrated margin into the tumor mass (CVF = 0.54–0.58). **B,** After surgical resection removes the central tumor mass, CVF is reduced to zero in the CSF-filled cavity, but tumor remains in the infiltrated margins known as the RTV. The responses to radiation treatment are either decreasing RTV as the infiltrating tumor is killed and the brain tissue reorganizes with CVF returning toward normal (**C**), or increasing RTV as the unresponsive tumor continues infiltrating and further disrupting normal packing, thereby decreasing CVF over a larger volume (**D**). The green filled hexagons are well-packed brain cells with a thin extracellular matrix (blue lines around green brain cells) and orange filled circles are neoplastic cells with a larger yellow extracellular matrix (yellow annulus around orange tumor cells).

Table 1. Demographics of the patient population in group 1 (decrease in RTV during chemoradiation) and group 2 (increase in RTV during chemoradiation) and overall survival

Group	Age in years (mean ± SD)	Gender (M:F)	Tumor grade	Number	Initial KPS	Repeat resections	Survival (days)
1	60 ± 10	5:6	IV	11	86 ± 11	4	469 ± 385
2	57 ± 7	6:3	IV	9	91 ± 8	5	514 ± 332

NOTE: No statistically significant differences were found.

radiation necrosis may also disrupt normal tissue and expand the volume of abnormal CVF, such radiation changes are only seen on a longer time scale following chemoradiation treatment.

Results

Table 1 shows the similar demographics for groups 1 and 2 including age, sex, initial KPS, number of repeated resections, and overall survival times that were not distinguishable statistically ($P > 0.1$). Three of the four *MGMT* methylation-positive subjects belonged to group 1 but numbers were too low to apply statistical comparisons based on genetic differences.

Figure 2 (left) shows axial partitions from the 3D TSC bioscales through the head of a representative patient prior to (Fig. 2A) and following (Fig. 2B) chemoradiation. The extent of the RTV in the left cerebral hemisphere is reduced with contraction of the resection cavity during chemoradiation treatment. The axial proton images, pre- and postintravenous gadolinium-based contrast before and after radiation treatment are shown in Fig. 2 (right). These proton images confirm the decrease in volume of the resection cavity. Although the thick enhancing margins are suspicious for residual tumor, such anatomic images provide no quantitative information about tumor response. Figure 3A shows two representative TSC partitions from Fig. 2 (left, last two partitions on right top row) on which the RTV was determined objectively (gray voxels surrounding the surgical cavity) using the tumor TSC filter (44 mmol/L < TSC < 80 mmol/L) to exclude the central CSF-filled surgical cavity and peripheral normal tissue. The histograms of the TSC values in the RTV and normal control tissue away from the treatment site are shown in Fig. 3B. The 44 mmol/L boundary (vertical dashed line) separating normal and tumor-infiltrated tissue defined the boundary threshold between normal and abnormal CVF. Although the control tissue (solid circles) shows a narrow distribution, the tumor (solid triangles) shows a much broader distribution, consistent with partial volume effects and heterogeneity in microstructure of tumor margins compared with normal brain tissue.

Table 2 shows groups 1 and 2 differences in changes in the bioscales of CVF, RTV, and TCK for the treatment site, time to disease progression, and CVF of control tissue away from the radiation treatment sites. Regression analyses of CVF in control regions across the multiple sessions of chemoradiation treatment for each patient in each group showed longitudinal stability (group 1: CVF = 0.81 ± 0.01; group 2: CVF = 0.82 ± 0.03) with no statistical difference ($P > 0.1$) across time for each patient and between groups. In contrast, the CVF values for the RTV (group 1: CVF = 0.57 ± 0.03; group 2: CVF = 0.53 ± 0.04) were statistically lower ($P < 0.001$) than those of normal regions for each and all patients. There were no significant ($P > 0.1$) differences in initial RTVs or in the linear regressions of change in RTV and TCK as a function of time to first progression (group 1: $R < 0.5$, $P > 0.1$; group 2: $R < 0.3$, $P > 0.1$) for either group despite differences reflected in the bioscales. Hence, despite group 2 having a statistically significant increase ($P < 0.0002$) in RTV and decreased ($P < 0.00005$) TCK compared with group 1, the difference in time-to-progression was not significant. The large variances in these bioscales reflect heterogeneity in tumor responses. The two groups show significant differences for the CVF ($P < 0.05$) within the

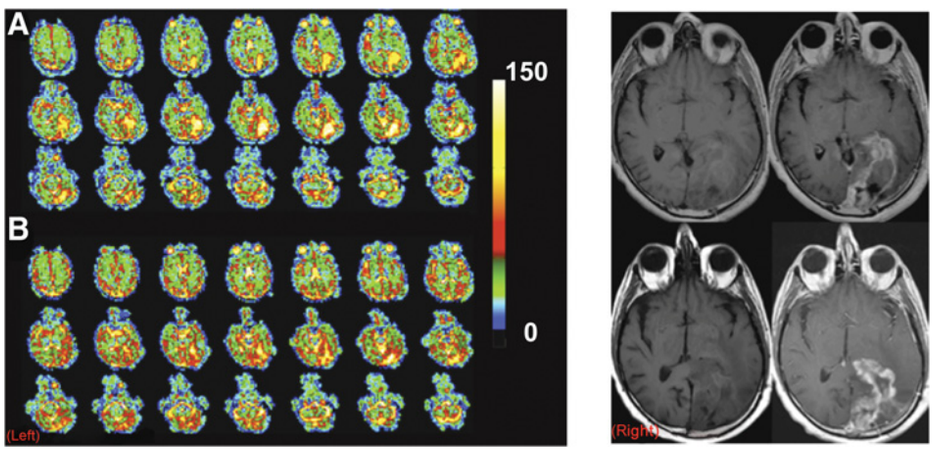

Figure 2.
Sodium and proton MRI of a representative patient with a resected glioblastoma in the inferior left temporo-occipital region. (Left) Axial partitions of the 3D TSC bioscale of a patient showing increased sodium concentration in the surgical resection site before (**A**) and after standard chemoradiation treatment (**B**). Color scale at right is in units of mmol/L. Note that two partitions on the far right on the top row of Fig. 1A and B are the partitions displayed in Fig. 3. (Right) T1-weighted images pre- (left column) and post- (right column) intravenous administration of gadolinium contrast for the same patient (top row) prior to and (bottom row) following chemoradiation treatment. The left cerebral hemisphere shows the surgical cavity filled with CSF and surrounding tissue with elevated TSC from tumor infiltration and edema. Radiation treatment shrinks the cavity, but the residual tumor persists in the margins.

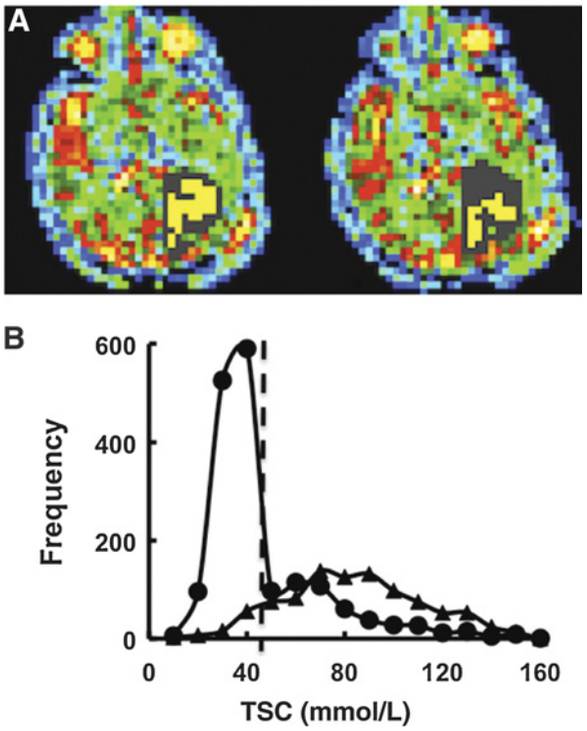

Figure 3.
Methodology of the sodium image analysis. **A,** Two representative axial partitions from the 3D TSC bioscale of the same patient as in Fig. 2 prior to radiation treatment showing the semiautomated selected RTV region (gray area) around the surgical cavity in the left temporo-occipital region. These two partitions are the same far right partitions on the top row of Fig. 1A and B. **B,** Histograms of TSC (mmol/L) in normal brain tissue (solid circles) and tumor (solid triangles) defined the boundary of the peripheral margin (44 mmol/L, two SDs from normal TSC = 34 mmol/L, vertical dashed line) of the RTV. The skew of the normal TSC distribution is due to the partial volume effect of voxels containing both tissue and CSF with the large voxel size (nominal $5 \times 5 \times 5$ mm^3) of the spherical projection acquisition used for quantitative sodium MR imaging at 3 Tesla.

tumor-infiltrated volumes. The negative value for fractional TCK for group 2 indicated tumor expansion with increases of the RTV during treatment.

Figure 4A shows regression plots of CVF during radiation treatment for 2 representative patients showing either statistically significant ($R > \pm 0.95$, $P < 0.04$) decrease (solid circles, dashed line) or increase (solid squares, dotted line) in CVF in the RTV compared with a stable CVF in normal tissue (open circles and squares, solid lines). The patient with a significant increase in CVF within the RTV showed decreasing RTV, whereas the patient with a decrease in CVF showed increasing RTV (Fig. 4B). Similar plots for all patients with significant changes in RTV are given in the Supplementary Materials and Methods (Supplementary Fig. S1).

Discussion

The continued abysmal prognosis of glioblastoma indicates that the current aggressive and costly trimodal treatment of surgery, radiation, and chemotherapy is inadequate for cure.

The results of this study indicate that fractionated chemoradiation has a widely variable effectiveness in destroying glioblastoma cells, which may be reflected in the widely variable survival times (group 1: 469 ± 385 days; group 2: 514 ± 332 days). The range of TCK varied greatly, from values as high as 80% for one patient (group 1: mean TCK = +31 ± 0.22%; mean RTV decrease = 34 ± 23%), whereas other tumors continued to grow increasing tumor volume by as much as almost 100% (group 2: mean TCK = −80 ± 66%; mean RTV increase = 98 ± 91%) across the 6 weeks of treatment. Changes in CVF, TCK, and RTV during fractionated chemoradiation were not correlated with patient prognosis, either as days of survival or in days to disease progression. This great variability is not a result of inaccurate measurement, as the control regions away from radiation treatment showed persistently accurate values with little biological variation (<1%) across the multiple studies of each patient and among patients. Rather, the large biological variances in the treatment region must reflect the highly variable responses of these tumors to treatment, possibly reflecting the heterogeneity in the four subtypes of glioblastoma (classical, mesenchymal, proneural, and neural) in this cohort. The genetic information was limited for this cohort and insufficient for statistical analysis.

The variability within the treatment volume, but not the control region during the 6-week treatment protocol suggests that these bioscales are responsive in real-time to biological processes occurring during fractionated chemoradiation. The temporal changes in the bioscales during radiation show consistent trends for individual patients indicating that the biological changes are monotonic and not random. The low efficiency of cell kill for many of the patients may explain the apparent lack of prognostic value of these parameters in this setting and is consistent with the poor outcome of glioblastoma. Presumably, subsequent events in the clinical course and in the variable genetics of the remaining tumor cells have greater impact on survival time than the fractionated chemoradiation. The repeated resections also reflect the poor response to this therapy.

The poor cell kill of tumor cells within the brain by fractionated chemoradiation is at odds with *in vitro* studies of cell suspensions

Table 2. Therapeutic responses in bioscales for groups 1 and 2 to chemoradiation as indicated by initial RTV, changes in RTV and CVF, fractional TCK, and time to first disease progression

Group	Brain region	CVF	Initial RTV (mL)	RTV Change (mL)	RTV Change (%)	Fractional TCK	Progression time (days; mean ± SD)
1	Tumor	0.57 ± 0.03[a]	47 ± 37	−17 ± 16[c]	−34 ± 23[c]	+0.31 ± 0.22[d]	205 ± 191
	Control	0.81 ± 0.01[b]	–	–	–	–	
2	Tumor	0.53 ± 0.04	37 ± 21	+39 ± 25[c]	+98 ± 91[c]	−0.80 ± 0.66[d]	283 ± 432
	Control	0.82 ± 0.03[b]	–	–	–	–	

[a]$P < 0.05$ for comparison of tumor CVF between groups 1 and 2.
[b]$P < 0.001$ for comparison of CVF of tumor to control within each group.
[c]$P < 0.0002$ for comparison of change in RTV between groups 1 and 2.
[d]$P < 0.00005$ for comparison of fractional TCK across chemoradiation for groups 1 and 2.

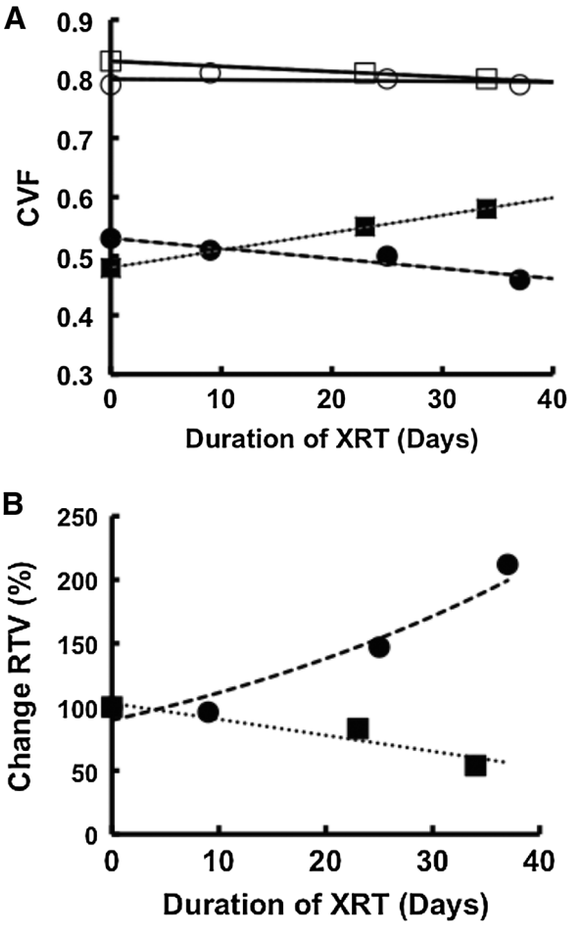

Figure 4.

Trends in CVF (**A**) and RTV (**B**) for treatment regions of 2 patients with responses that show statistically significant ($R > \pm 0.95$, $P < 0.04$) increases (solid squares, dotted line) and decreases (solid circles, dashed line) in CVF during chemoradiation treatment, whereas the control regions remain stable (open squares and circles, solid lines). These patients showed significant inverse responses between RTV and CVF, matching the model in Fig. 1. The patient with the decrease in CVF had an increasing RTV and a survival time of 344 days. The patient with an increasing CVF and decreasing RTV returning toward normal values had a longer survival time of 547 days. These patients were of similar age with similar sized glioblastomas initially, but showed very different responses and survival under the same treatment protocol.

where even low-dose radiation is effective. This difference in efficiency supports the need for *in vivo* measurements to understand therapeutic response. Clinical trials often use global outcome measures of survival to compare different treatment arms. Bioscales that assess the treatment efficiency in real-time may provide a more economically favorable outcome measure, not only by shortening clinical trials but also for management of individual patients. The goal is to maximize TCK while normalizing CVF within the RTV for each patient. Treatment response can be monitored for each patient rather than employing the surveillance approach as in current practice. Treatments can be changed rapidly when a particular treatment fails to yield a favorable response (low TCK, increasing RTV, decreasing CVF) for a specific patient. Such personalized management should be more effective than using population-based protocols from clinical trials.

Limitations of this study include the small number of patients, limited by funding that restricted recruitment to 3 years so that 3-year survival follow-up data would be available. Bioscales were measured only during the 6 weeks of chemoradiation, whereas longer term quantitative sodium MRI, perhaps at the same time as the first follow-up proton clinical MRI may have been informative. These bioscales were not corrected for partial volume effects despite the low spatial resolution. However, such blurring of bioscale values is unlikely to result in the observed heterogeneous results. Patient tolerance of multiple MRI examinations during the already arduous commitment to fractionated chemoradiation treatment was variable. This may be of less concern if such imaging became a routine part of clinical practice, especially if an ineffective therapy was shortened. The specific genetics of the glioblastomas were not available for this cohort. The sodium-based bioscales were not compared with perfusion MRI parameters that have long been reported as being a useful indicator of tumor progression (28–30) as this modality is not used clinically during treatment.

The addition of radiation to gross total resection increased survival from 3–4 months to 7–12 months (5) and the addition of temozolomide chemotherapy further increased median survival to about 14.6 months (31). As the follow-up chemotherapy increased survival times significantly, the lack of survival prediction based on early fractionated chemoradiation responsiveness measured by the sodium bioscales is not surprising. The fact that the bioscales are sensitive to radiation-induced tumor responses during treatment, including continued growth, suggests that these bioscales should be examined for real-time responses of subsequent chemotherapy. Such real-time responses could be used in individual patient management as well as in clinical trials of new treatments and for other tumor types.

An important aspect of this study is that the quantitative sodium MRI was performed on a busy clinical service by clinical MR technologists using a clinical 3T scanner, indicating that such measurements can be performed in a clinical environment without specialized personnel, once the hardware and software are made available.

Disclosure of Potential Conflicts of Interest

T.A. Chan has ownership interests (including patents) in Gritstone Oncology and An2H, is a consultant/advisory board member for Bristol-Myers Squibb, An2H, AstraZeneca, Illumina, and reports receiving commercial research grants from Bristol-Myers Squibb, AstraZeneca, Illumina, Pfizer, and An2H. Y. Yamada reports receiving speakers bureau honoraria from BrainLab, Varian Medical Systems, Institute for Medical Education, and Vision RT. No potential conflicts of interest were disclosed by the other authors.

Authors' Contributions

Conception and design: K.R. Thulborn, A. Lu, M. Pauliah, K. Beal
Development of methodology: K.R. Thulborn, A. Lu, I.C. Atkinson, M. Pauliah
Acquisition of data (provided animals, acquired and managed patients, provided facilities, etc.): K.R. Thulborn, A. Lu, I.C. Atkinson, M. Pauliah, K. Beal, T.A. Chan, A.M.P. Omuro, Y. Yamada, M.S. Bradbury
Analysis and interpretation of data (e.g., statistical analysis, biostatistics, computational analysis): K.R. Thulborn, I.C. Atkinson, M. Pauliah, T.A. Chan, A.M.P. Omuro, Y. Yamada, M.S. Bradbury
Writing, review, and/or revision of the manuscript: K.R. Thulborn, A. Lu, M. Pauliah, K. Beal, T.A. Chan, A.M.P. Omuro, Y. Yamada, M.S. Bradbury
Administrative, technical, or material support (i.e., reporting or organizing data, constructing databases): K.R. Thulborn, A. Lu, M. Pauliah, T.A. Chan

Study supervision: K.R. Thulborn, A. Lu, M. Pauliah, T.A. Chan, M.S. Bradbury
Other (principal investigator of NIH RO1 grant that funded this study): K.R. Thulborn

Acknowledgments

The authors acknowledge financial grant support from PHS NIH RO1 CA1295531A1.

The costs of publication of this article were defrayed in part by the payment of page charges. This article must therefore be hereby marked *advertisement* in accordance with 18 U.S.C. Section 1734 solely to indicate this fact.

Received June 30, 2018; revised October 4, 2018; accepted November 16, 2018; published first November 28, 2018.

References

1. McLendon RE, Halperin EC. Is the long-term survival of patients with intracranial glioblastoma multiforme overstated? Cancer 2003;98:1745–8.
2. Mineo JF, Bordron A, Baroncini M, Ramirez C, Maurage CA, Blond S, et al. Prognosis factors of survival time in patients with glioblastoma multiforme: a multivariate analysis of 340 patients. Acta Neurochir 2007; 149:245–52.
3. Lacroix M, Abi-Said D, Fourney DR, Gokaslan ZL, Shi W, DeMonte F, et al. A multivariate analysis of 416 patients with glioblastoma multiforme: prognosis, extent of resection, and survival. J Neurosurg 2001;95:190–8.
4. Verhaak RG, Hoadley KA, Purdom E, Wang V, Qi Y, Wilkerson MD, et al. Cancer Genome Atlas Research Network. Integrated genomic analysis identifies clinically relevant subtypes of glioblastoma characterized by abnormalities in PDGFRA, IDH1, EGFR, and NF1. Cancer Cell 2010;17: 98–110.
5. Young RM, Jamshidi A, Davis G, Sherman JH. Current trends in the surgical management and treatment of adult glioblastoma. Ann Transl Med 2015;3:121.
6. Giese A, Bjerkvig R, Berens ME, Westphal M. Cost of migration: invasion of malignant gliomas and implications for treatment. J Clin Oncol 2003;21: 1624–36.
7. Eidel O, Burth S, Neumann JO, Kieslich PJ, Sahm F, Jungk C, et al. Tumor infiltration in enhancing and non-enhancing parts of glioblastoma: a correlation with histopathology. PLoS One 2017;12:e0169292.
8. Grabowski MM, Recinos PF, Nowacki AS, Schroeder JL, Angelov L, Barnett GH, et al. Residual tumor volume versus extent of resection: predictors of survival after surgery for glioblastoma. J Neurosurg 2014;121:1115–23.
9. Xie Q, Mittal S, Berens ME. Targeting adaptive glioblastoma: an overview of proliferation and invasion. Neuro Oncol 2014;16:1575–84.
10. Iacob G, Dinca EB. Current data and strategy in glioblastoma multiforme. J Med Life 2009;2:386–93.
11. Feinberg DA, Crooks LA, Kaufman L, Brant-Zawadzki M, Posin JP, Arakawa M, et al. Magnetic resonance imaging performance: a comparison of sodium and hydrogen. Radiology 1985;156:133–8.
12. Hilal SK, Maudsley AA, Ra JB, Simon HE, Roschmann P, Wittekoek S, et al. *In vivo* NMR imaging of sodium-23 in the human head. J Comput Assist Tomogr 1985;9:1–7.
13. Perman WH, Turski PA, Houston LW, Glover GH, Hayes CE. Methodology of *in vivo* human sodium MR imaging at 1.5 T. Radiology 1986; 160:811–20.
14. Turski PA, Houston LW, Perman WH, Hald JK, Turski D, Strother CM, et al. Experimental and human brain neoplasms: detection with *in vivo* sodium MR imaging. Radiology 1987:163:245–9.
15. Ra JB, Hilal SK, Oh CH, Mun IK. *In vivo* magnetic resonance imaging of sodium in the human body. Magn Reson Med 1988;7:11–22.
16. Perman WH, Thomasson DM, Bernstein MA, Turski PA. Multiple short-echo (2.5-ms) quantitation of *in vivo* sodium T2 relaxation. Magn Reson Med 1989;9:153–60.
17. Thulborn KR. Clinical rationale for very high field (3.0 Tesla) functional MR imaging. Topics Magn Reson Imaging 1999;10:37–50.
18. Boada FE, Gillen JS, Shen GX, Chang SY, Thulborn KR. Fast three dimensional sodium imaging. Magn Reson Med 1997;37:706–15.
19. Thulborn KR, Atkinson IC. From standardization to quantification: beyond biomarkers towards bioscales as neuro MR imaging surrogates of clinical endpoints. AJNR Am J Neuroradiol 2013;34:2241–9.
20. Christensen JD, Barrère BJ, Boada FE, Vevea JM, Thulborn KR. Quantitative tissue sodium concentration mapping of normal rat brain. Magn Reson Med 1996;36:83–9.
21. Thulborn KR, Davis D, Adams H, Gindin T, Zhou J. Quantitative tissue sodium concentration mapping of the growth of focal cerebral tumors with sodium magnetic resonance imaging. Magn Reson Med 1999;41:351–9.
22. Thulborn KR. Quantitative sodium MR imaging: a review of its evolving role in medicine. Neuroimage 2018;168:250–68.
23. Thulborn K, Lui E, Guntin J, Jamil S, Sun Z, Claiborne TC, et al. Quantitative sodium MRI of the human brain at 9.4 T provides assessment of tissue sodium concentration and cell volume fraction during normal aging. NMR Biomed. 2016;29:137–43.
24. Lu A, Atkinson IC, Claiborne TC, Damen FC, Thulborn KR. Quantitative sodium imaging with a flexible twisted projection pulse sequence. Magn Reson Med 2010;63:1583–93.
25. Atkinson IC, Lu A, Thulborn KR. Preserving the accuracy and resolution of the sodium bioscale from quantitative sodium MRI during intra-subject alignment across longitudinal studies. Magn Reson Med 2012;68:751–61.
26. Wallner KE, Galicich JH, Krol G, Arbit E, Malkin MG. Patterns of failure following treatment for glioblastoma multiforme and anaplastic astrocytoma. Int J Radiat Oncol Biol Phys 1989;16:1405–9.
27. Bruehlmeier M, Roelcke U, Bläuenstein P, Missimer J, Schubiger PA, Locher JT, et al. Measurement of the extracellular space in brain tumors using 76Br-bromide and PET. J Nucl Med 2003;44:1210–8.
28. Siegal T, Rubinstein R, Tzuk-Shina T, Gomori JM. Utility of relative cerebral blood volume mapping derived from perfusion magnetic resonance imaging in the routine follow up of brain tumors. J Neurosurg 1997:86:22–7.
29. Hu LS, Eschbacher JM, Heiserman JE, Dueck AC, Shapiro WR, Liu S, et al. Reevaluating the imaging definition of tumor progression: perfusion MRI quantifies recurrent glioblastoma tumor fraction, pseudoprogression, and radiation necrosis to predict survival. Neuro Oncol 2012;14:919–30.
30. Gasparetto EL, Pawlak MA, Patel SH, Huse J, Woo JH, Krejza J, et al. Posttreatment recurrence of malignant brain neoplasm: accuracy of relative cerebral blood volume fraction in discriminating low from high malignant histologic volume fraction. Radiology 2009;250:887–96.
31. Stupp R, Mason WP, van den Bent MJ, Weller M, Fisher B, Taphoorn MJ, et al. European organisation for research and treatment of cancer brain tumor and radiotherapy groups; national cancer institute of Canada clinical trials group. Radiotherapy plus concomitant and adjuvant temozolomide for glioblastoma. N Engl J Med 2005;352:987–96.